



Neural activity promotes long distance, target-specific regeneration of adult retinal axons

Citation

Lim, Jung-Hwan A., Benjamin K. Stafford, Phong L. Nguyen, Brian V. Lien, Chen Wang, Katherine Zukor, Zhigang He, and Andrew D. Huberman. 2017. "Neural activity promotes long distance, target-specific regeneration of adult retinal axons." *Nature neuroscience* 19 (8): 1073-1084. doi:10.1038/nn.4340. <http://dx.doi.org/10.1038/nn.4340>.

Published version

<https://doi.org/10.1038/nn.4340>

Link

<http://nrs.harvard.edu/urn-3:HUL.InstRepos:34493051>

Terms of use

This article was downloaded from Harvard University's DASH repository, and is made available under the terms and conditions applicable to Other Posted Material (LAA), as set forth at

<https://harvardwiki.atlassian.net/wiki/external/NGY5NDE4ZjgzNTc5NDQzMGIzZWZhMGFIOWI2M2EwYTg>

Accessibility

<https://accessibility.huit.harvard.edu/digital-accessibility-policy>

Share Your Story

The Harvard community has made this article openly available. Please share how this access benefits you. [Submit a story](#)



Published in final edited form as:

Nat Neurosci. 2016 August ; 19(8): 1073–1084. doi:10.1038/nn.4340.

Neural activity promotes long distance, target-specific regeneration of adult retinal axons

Jung-Hwan A. Lim¹, Benjamin K. Stafford², Phong L. Nguyen², Brian V. Lien¹, Chen Wang³, Katherine Zukor⁴, Zhigang He³, and Andrew D. Huberman^{5,6,*}

¹Division of Biological Sciences, University of California, San Diego

²Department of Neurosciences, School of Medicine, University of California, San Diego

³Boston Children's Hospital and F.M. Kirby Neurobiology Center, Harvard Medical School

⁴Animal, Dairy and Veterinary Sciences Department, Utah State University

⁵Department of Neurobiology, Stanford University School of Medicine

⁶Department of Ophthalmology, Stanford University School of Medicine

Abstract

Axons in the mammalian central nervous system (CNS) fail to regenerate after injury. Here we show that if retinal ganglion cell (RGC) activity is increased by visual stimulation or using chemogenetics, their axons regenerate. We also show that if enhancement of neural activity is combined with elevation of the cell growth-promoting pathway involving mammalian target of rapamycin (mTOR), RGC axons regenerate the long distances necessary to re-innervate the brain. Analysis of genetically-labeled RGCs revealed this regrowth can be target specific: RGC axons navigated back to their correct visual targets and avoided targets incorrect for their function. Moreover, these regenerated connections were successful in partially rescuing a subset of visual behaviors. Our findings indicate that combining neural activity with activation of mTOR can serve as powerful tool for enhancing axon regeneration and they highlight the remarkable capacity of CNS neurons to re-establish accurate circuit connections in the adult brain.

Neurons in the adult mammalian central nervous system (CNS) fail to regenerate after injury thereby preventing recovery of numerous CNS functions¹. A major goal of neuroscience is to identify the factors that limit CNS regeneration and devise therapeutic strategies to overcome them. Previous work illustrated that factors inherent to the mature CNS environment are unfavorable for axon growth but that damaged CNS axons are capable of

Users may view, print, copy, and download text and data-mine the content in such documents, for the purposes of academic research, subject always to the full Conditions of use:http://www.nature.com/authors/editorial_policies/license.html#terms

Correspondence to: adh1@stanford.edu.

Author Contributions

J. Lim carried out all experiments, imaging, analysis of the data, and figure preparation. B. Stafford performed recordings from RGCs and the analysis of activity in response to chemical genetic manipulations. P. Nguyen assisted with the visual stimulation experiments, tissue collection, and provided technical assistance. B. Lien contributed to the visual stimulation experiments and tissue collection. C. Wang prepared AAV-cRheb1 viruses. K. Zukor provided technical assistance for optic nerve crush surgery and AAV-cRheb1. Z. He provided AAV-cRheb1 virus. A. Huberman supervised the project and data analyses. J. Lim, Z. He, B. Stafford, and A. Huberman wrote the paper.

regenerating through peripheral nerve grafts². Subsequent work identified some of the CNS factors responsible for inhibiting axon regrowth including myelin associated proteins^{3,4}, reactive glial scarring⁵, up-regulation of extracellular matrix factors⁶, and repellent guidance cues^{7,8}. Factors intrinsic to CNS neurons also prevent axonal regeneration. For example, during development, CNS neurons down-regulate expression of growth-promoting molecules⁹. Some CNS axon regeneration can be achieved by augmenting intrinsic cell growth-promoting factors such as mammalian-target-of-rapamycin (mTOR), cyclic-adenosine-monophosphate (cAMP) or ciliary-neurotrophic-factor (CNTF)¹⁰⁻¹², or by down-regulating transcriptional inhibitors of axon growth such as Kruppel-like Factor 4 (KLF4)¹³ or suppressor-of-cytokine-signaling-3 (SOCS3)¹⁴. In general, it is thought that both extrinsic and intrinsic factors limit CNS axon regeneration¹⁵.

The eye-to-brain pathway consisting of retinal ganglion cell (RGC) connections to subcortical targets is a widely used model for studying vertebrate CNS regeneration^{2,10,13,16}. After optic nerve crush (ONC), RGC axons fail to regenerate beyond the crush site, and eventually the RGCs die altogether¹⁷. Recent work showed that increasing mTOR signaling in RGCs by deletion of one of its inhibitors, phosphatase-and-tensin-homolog (PTEN), allows a significant number of RGCs to regenerate their axons through lesions in the optic nerve¹⁰, an effect that is further enhanced by deletion of SOCS3¹⁸. However, neither PTEN deletion nor combined PTEN/SOCS3 deletion stimulated RGC axon regeneration back into the brain. Instead, the regenerating RGC axons stall at the optic chiasm¹⁰ or steer away from the brain and travel up the opposite optic nerve^{18,19}, leaving RGCs divorced from their central targets.

The purpose of this study was twofold. First, we sought to identify strategies that alone or in combination would allow adult RGC axons to regenerate after ONC, into and through the optic chiasm and back to the brain. We find that, if neural activity is enhanced along with levels of mTOR, RGC axons re-innervate their targets, including the most distal subcortical visual nuclei. That discovery, in turn, allowed us to address a second major question: whether regenerating RGC axons have the ability to reconnect with their correct targets, and restore visual function. Together, our data support the combined use of neural activity and molecular programs for intrinsic growth as strategies to regenerate visual circuits. Our results reveal the remarkable ability of adult CNS neurons to re-establish correct patterns of connectivity following injury.

Results

Enhancement of RGC axon regeneration by visual stimulation

We lesioned RGC axons by crushing the optic nerve just posterior to the orbit of the eye using fine forceps (Fig. 1a). Three weeks later we labeled RGCs and their axons with intravitreal injections of cholera-toxin-subunit- β (CT β) conjugated to Alexa-Fluor-594 (CT β -594) (Fig. 1a, 1c, 1d). In the absence of any therapeutic intervention, very few RGC axons extend beyond the crush site (Fig. 1d) ('Group 1') (control group details in Supplementary Fig. 1) and the majority of RGCs die (Supplementary Fig. 2). This 'regenerative failure' is consistent with hundreds of previous reports spanning many decades¹⁵. An earlier study showed that electrically stimulating developing RGCs *in vitro*

accelerated outgrowth of their axons²⁰. This inspired us to investigate whether enhancing the electrical activity of adult RGCs would promote regeneration of their axons *in vivo*. Vision is a potent stimulus for driving the electrical activity of RGCs. Thus, we examined whether exposing adult mice to high contrast visual stimulation daily for three weeks following ONC, would trigger regeneration of RGC axons (schematized in Fig. 1b and 1c) (see methods). This paradigm was effective in causing some RGC axons to regenerate a short distance past the lesion site (Fig. 1e) ('Group 2'), an effect that, while relatively limited in distance, was statistically significant compared to controls (Fig. 1f).

To further explore the influence of neural activity on axon regeneration we employed 'chemogenetic' technology²¹. First we tested whether reducing RGC activity would block the enhancement of RGC axon growth caused by visual stimulation. We overexpressed the engineered G-protein-coupled-receptor hM4Di [Gi/o-coupled human muscarinic M₄ designer receptor exclusively activated by a designer drug (DREADD)]²¹ in RGCs by injecting mice with adeno-associated-virus AAV2-hM4Di-mCitrine in one eye *in vivo* (Fig. 2a and 2b). Two weeks later, hM4Di-mCitrine expressing cells were observed throughout the RGC layer (Supplementary Fig. 3a-3d). They also expressed the marker RBPMS²², confirming them as RGCs (not shown). When exposed to the synthetic ligand clozapine-N-oxide (CNO), hM4Di causes membrane hyperpolarization and silencing of CNS neurons²¹. We confirmed this in RGCs by targeting the AAV2-hM4Di-mCitrine-infected RGCs for whole-cell current-clamp recordings of their responses to current injections and high contrast visual stimulation (Fig. 2c and Supplementary Fig. 4a-4d). In the absence of CNO, expression of AAV2-hM4Di-mCitrine had no impact on RGC activity. Application of CNO, however, led to strong hyperpolarization and suppression of RGC spiking in response to current injection and visual stimulation (Fig 2c and Supplementary Fig. 4a-4d).

Next we applied the hM4Di strategy to test whether suppression of RGC activity impacts the axon regeneration caused by daily visual stimulation. We injected AAV-hM4Di-mCitrine into one eye, waited 2 weeks for expression, then crushed the same eye's optic nerve and systemically administered the mice CNO twice a day for three weeks, while also exposing the animals to high contrast visual stimulation to drive RGC firing (Fig. 2d). Reducing RGC activity with hM4Di/CNO abolished the effect of visual stimulation on RGC axon regeneration and also reduced the total number of CT β -labeled RGC axons anterior to the lesion site (compare Fig. 2e and 2e1 with Fig. 1e and 1e1) (Fig. 2k). These findings suggest that high contrast visual stimulation promotes regeneration of RGC axons by increasing their overall levels of electrical activation. The reduced number of CT β -labeled RGC axons anterior to the lesion site observed in mice that received hM4Di/CNO treatments also suggests that neural activity may impact the number of RGCs that survive optic nerve damage.

Next we tested whether chemogenetically increasing levels of RGC activity can promote their axons to regenerate. We overexpressed the CNO-sensitive synthetic receptor, hM3Dq (G_q-coupled human muscarinic M₃ DREADD)²¹ in RGCs by intravitreal injections of AAV2-hM3Dq-mCitrine (Fig. 2f and 2g). Two weeks post-injection, expression of hM3Dq-mCitrine was observed in all four quadrants of the RGC layer (Supplementary Fig. 3e-3h) and co-labeling of these retinas with RBPMS²² showed that >90% of RGCs expressed the

hM3Dq (Supplementary Fig. 3i-3l). In whole-mount retinas from these mice, CNO-driven activation of the hM3Dq receptor caused a significant increase in the number of spikes elicited from infected RGCs by current injection or by high contrast visual stimulation (Fig. 2h and Supplementary Fig. 4e-4h).

What is the impact of chemogenetically enhancing neural activity on RGC axon regeneration? To test this, we injected a group of mice with AAV2-hM3Dq-mCitrine, crushed the optic nerve two weeks later, and administered CNO twice a day for three weeks (Fig. 2f and 2i). To isolate the effects of hM3Dq-driven RGC activity, these mice were housed on normal light-dark cycles, with no additional visual stimulation. CT β labeling of RGC axons at the end of the 3-week chemogenetic stimulation period revealed that hM3Dq/CNO treatments led to a greater degree of RGC axon regeneration (Fig. 2j-2k) compared to control mice ('Group 1'), or to mice that underwent daily visual stimulation alone ('Group 2') (Fig. 2k). A large number of hM3Dq-treated RGC regrew their axons through the lesion site in the proximal nerve and indeed, some even extended into mid optic nerve (Fig. 2j; and see j2'). These results indicate that elevating RGC spiking levels is sufficient to promote axon regeneration and support the idea that visual stimulation exerts its influence on RGC axon regeneration by increasing levels of activity.

Synergistic effects of visual stimulation and mTOR elevation

Previous studies showed that increasing mTOR signaling by deletion of one of its repressors, PTEN, can trigger RGC axon regeneration^{10,16,18,19}. Here we tested whether expressing a positive regulator of mTOR signaling –ras-homolog-enriched-in-brain 1 (Rheb1) protein–also could promote regeneration. We injected AAV overexpressing constitutively active Rheb1 (AAV2-cRheb1)²³ into one eye of adult mice, waited two weeks for cRheb1 overexpression, then crushed the optic nerve of the AAV-injected eye. Three weeks later, we labeled RGC axons by intravitreal injection of CT β -594 and assessed their regeneration (Fig. 3a) (see methods). Injections of AAV2-cRheb1 significantly increased the number of cells in the adult RGC layer that express phosphorylated S6 ribosomal protein (p-S6), a downstream marker of phosphorylated mTOR activity (Fig. 3b–3d) (Supplementary Fig. 5).

Overexpression of cRheb1 enhanced the ability of adult RGCs to regenerate their axons after injury. Three weeks post ONC, we observed RGC axons extending through the lesion site and into the proximal optic nerve (Fig. 3e) ('Group 3'), an effect that was statistically significant compared to control mice receiving either i) no treatment, ii) intravitreal injections of saline or iii) injections of a control virus (AAV2-Cre) (collectively, 'Group 1') (Fig. 3g) (Supplementary Fig. 1). The effects of AAV2-cRheb1 on RGC axon regeneration were attenuated by chronic administration of the mTOR inhibitor, rapamycin (Supplementary Fig. 6), supporting the idea that the effect of AAV2-cRheb1 stemmed from elevation of the mTOR signaling pathway. Although there were quantitative differences in the overall number of axons that regenerated in response to cRheb1 overexpression versus visual stimulation versus PTEN deletion (ref:¹⁰ and Supplementary Fig. 7) the general patterns of regeneration observed in these three groups were similar: RGC axons regenerated past the lesion site but failed to grow the full distance of the optic nerve to reach the optic chiasm or brain (Fig. 3e and 3g) (Supplementary Fig. 7).

Next, we tested whether combining visual stimulation with enhanced mTOR signaling would increase the distance that RGC axons regenerate beyond that observed with either treatment alone. We injected one eye with AAV2-cRheb1 then allowed two weeks for elevation of mTOR signaling in RGCs. We then crushed the optic nerve and exposed the mice to high contrast visual stimulation daily for three weeks (Supplementary Fig. 8a) ('Group 5'). In these mice, RGC axons regenerated past the lesion site but failed to extend beyond the mid optic nerve and optic chiasm (Supplementary Fig. 8a; Supplementary Fig. 9a).

In the motor system, forced use of an impaired limb promotes sprouting of corticospinal axons²⁴. We therefore tested whether, after treatment with AAV2-cRheb1 and crushing one optic nerve, suturing shut the eye corresponding to the non-lesioned optic nerve could further enhance RGC axon regeneration of the lesioned eye pathway ('Group 6'). Biased use of the lesioned eye pathway in this manner enhanced RGC axon regeneration compared to 'Group 3' mice treated with AAV2-cRheb1 alone (Supplementary Fig. 8b; Supplementary Fig. 9a). However, if these mice were also exposed to high contrast visual stimulation every day for three weeks (Fig. 3f and Supplementary Figs. 10-12) ('Group 4'), this combination of treatments (hereafter referred to as 'biased-visual-stimulation/AAV2-cRheb1') triggered long-distance regeneration of RGC axons. In 7 of 10 mice treated in this manner, RGC axons regenerated through the ONC site, down the full length of the optic nerve and into the optic chiasm (Fig. 3f; 3f1-3f4; Supplementary Figs. 10-12), an effect that was highly significant compared to control mice ('Group 1'), to mice that received AAV2-cRheb1 treatment ('Group 3') (Fig. 3g), or to mice that received visual stimulation/AAV2-cRheb1 but that had both eyes open ('Group 5'). Also, when we sutured shut the lesioned/AAV2-cRheb1 treated eye, the number of RGC axons that regenerated was similar to that of the 'Group 3' animals that received AAV2-cRheb1 treatment and importantly, no axons made it to the optic chiasm (Supplementary Fig. 8c; Supplementary Fig. 9a) ('Group 7').

We found that the effect of the combined treatments also relied critically on cRheb1 overexpression of the RGCs. When the daily visual stimulation was biased toward the lesioned-eye-pathway but we did not overexpress cRheb1, the number of RGC axons that regenerated was dramatically reduced (Supplementary Fig. 8d; quantified in Supplementary Fig. 9b) ('Group 8'). Further, in the absence of cRheb1 overexpression and visual stimulation, the number of regenerated RGC axons was significantly reduced (Supplementary Fig. 8e; quantified in Supplementary Fig. 9b) ('Group 9'). This highlights the need for elevating intrinsic growth programs missing in mature RGCs⁹⁻¹².

Together, the different combinations of treatments we designed to promote regeneration highlight the importance of providing visual stimulation to the AAV2-cRheb1 treated eye and they argue against indirect effects of the biased-visual-stimulation/AAV2-cRheb1 protocol on non-visual factors such as enhanced locomotion (Fig. 3 and Supplementary Figs. 8-12). We considered whether the enhanced axon regeneration we observed in mice given biased visual stimulation/AAV2-cRheb1 reflected an increase in RGC survival. Indeed, the number of RGCs surviving ONC more than doubled in the biased-visual-stimulation/AAV2-cRheb1 group (Supplementary Fig. 13). The most parsimonious conclusion from all these experiments is that it is the combination of simultaneously enhancing activity and enhancing

mTOR signaling that allows a set of RGC axons to regenerate through lesion sites and extend long distances down the optic nerve.

Long-range RGC axon regeneration to targets in the brain

A critical milestone for the re-establishment of functional eye-to-brain circuits is long-distance regeneration of RGC axons back to the brain. The retinofugal pathway includes several dozen target nuclei located in the fore- and midbrain (Fig. 4c and Supplementary Fig. 14)²⁵. In mice receiving biased-visual-stimulation/AAV2-cRheb1 treatments ('Group 4') (Fig. 4a-4c), regenerated CT β -labeled RGC axons were observed in multiple subcortical visual targets (Fig. 4d-4p). 7 of 10 mice that received the biased-visual-stimulation/AAV2-cRheb1 treatments exhibited RGC axons that regenerated past the ONC site, through the optic chiasm and optic tract, and back to visual targets in the brain (Fig. 4d-4p) (Supplementary Fig. 15) (Table 1). Three weeks after nerve crush, CT β -labeled RGC axons were observed in the most proximal visual target, the hypothalamic suprachiasmatic nucleus (SCN) (Fig. 4d and 4k), and in the thalamic ventral lateral geniculate nucleus (Fig. 4e and 4l) and dorsal lateral geniculate nucleus (Fig. 4f and 4m) (vLGN and dLGN, respectively). Regenerated RGC axons were also observed in midbrain pretectal nuclei such as the olivary pretectal nucleus (OPN) (Fig. 4g and 4n) and posterior limitans (Fig. 4h), and in accessory optic targets of the brainstem, such as the medial terminal nucleus (MTN) (Fig. 4i and 4o). Remarkably, RGC axons were also detected in the subcortical visual target located furthest from the eye, the superior colliculus (SC) (Fig. 4j and 4p). Notably, we did not observe any CT β -labeled RGC axons in non-visual subcortical regions such as the somatosensory or auditory thalamus (not shown), indicating that regenerating RGC axons appropriately confine their trajectories to the retinofugal pathway. The extent of RGC axon regeneration along the retinofugal pathway and within each target varied from one mouse to the next (Table 1). Nevertheless, in every animal receiving biased-visual-stimulation/AAV2-cRheb1 treatment, the extent of regeneration was dramatic compared to mice treated only with AAV2-cRheb1 ('Group 3') or that received only visual stimulation but not AAV2-cRheb1 ('Group 2') (Figs. 1 and 3) (Table 1).

To ensure that the CT β -labeled axons we observed in the optic nerve and brain were regenerated axons and not spared RGC axons, we carried out several control experiments. For the first set of controls, we labeled RGC axons by intravitreal injections of CT β -594, and two days later we crushed the optic nerve. Then we waited one week, at which time we re-labeled all RGC axons by intravitreal injection of CT β -488 (Supplementary Fig. 16b). In every mouse examined, CT β -594 labeled axons were observed in the vicinity of the lesion site but never at the distal nerve or optic chiasm (Supplementary Fig. 16c; compare with non-lesioned CT β -594 labeled axons in Supplementary Fig. 16a), indicating that the ONC indeed caused RGC axons to degenerate. Additionally, RGC axons labeled after the ONC with CT β -488 were observed posterior to the eye and in the vicinity of the lesion site, but never in the mid- or distal optic nerve, optic chiasm or brain (Supplementary Fig. 16c) (not shown). These results support the conclusion that the ONC procedure did not spare RGC axons.

As a second set of controls, we tested whether biased-visual-stimulation/AAV2-cRheb protocol induced RGC axons to regenerate down the optic nerve in a time-dependent manner, which would not occur if the crush procedure had spared RGC axons. For these experiments, we allowed the mice a period of either 1 or 2 weeks for RGC axons to regenerate before assessing the distance of axon growth (Supplementary Fig. 17a). In mice provided one-week survival post-crush for regeneration to occur, RGC axons extended through and beyond the lesion site (Supplementary Fig. 17b), but were never observed in the distal nerve or within central visual targets (Supplementary Fig. 18a-18d). In mice allowed two weeks for regeneration to occur, there were an even greater number of RGC axons growing through the lesion site (Supplementary Fig. 17c-17d); some RGC axons were observed in the mid and distal optic nerve but no axons were observed in the chiasm or the brain (Supplementary Fig. 17c-17d). Only in mice treated with biased-visual-stimulation/AAV2-cRheb1 and allowed a minimum of 3 weeks for regeneration did we observe RGC axons regenerating through the optic chiasm and back into the brain (Figs. 3 and 4).

Together, these two sets of control experiments support the conclusion that our nerve crush procedure did not spare RGC axons. Rather, the CT β -labeled profiles observed in the optic nerve, chiasm and brain represent RGC axons that re-grew in a time-dependent manner through and beyond the crush site.

Target-specific axon regeneration in the brain

A critical unresolved issue in the field of CNS regeneration is whether re-growing axons can find and reconnect to their correct targets. The growth of RGC axons back into the brain we observed in mice receiving biased-visual-stimulation/AAV2-cRheb1 treatment (Figs. 3 and 4), provided us the opportunity to address this issue. Mammals, including mice and humans, have ~30 types of RGCs²⁵, each of which responds to a particular feature in the visual world and connects to a small subset of the 40+ retinorecipient targets. Different groups have discovered and characterized various transgenic mouse lines, each harboring green fluorescent protein (GFP) in specific RGC types^{25,26}. When combined with the axon-regrowth protocol described above, these mice offer the powerful opportunity to explore the specificity of RGC axon regeneration. Others have shown that mTOR-induced regeneration is biased toward alpha RGC types²⁷. We made use of a new mouse line: Cochlin-GFP (CoCH-GFP). In these mice many of the GFP-expressing RGCs are alpha RGCs (Supplementary Fig. 19) and we tested whether GFP⁺ RGCs regenerated their axons back to their correct targets in the brain.

In normal unlesioned mice, CoCH-GFP⁺ RGC axons densely innervate the vLGN, dLGN, OPN, and SC, and they avoid the SCN, MTN and intergeniculate leaflet (IGL) (Fig. 5c and Supplementary Fig. 19). In optic-nerve-lesioned CoCH-GFP mice treated with biased-visual-stimulation/AAV2-cRheb1 (Fig. 5a and 5b), a subset of the CT β -594⁺ axons in the optic nerve also expressed CoCH-GFP (Supplementary Fig. 20) indicating they indeed are part of the regenerating cohort. CT β -594 labeled RGC axons were observed in various retinorecipient targets in the brain, including the SCN, vLGN, dLGN, MTN, and SC (Fig. 5d-5m and 5p-5v). Remarkably, the only targets that contained axons that were double-labeled with CT β -594 *and* CoCH-GFP (i.e., regenerated CoCH-GFP⁺ RGC axons) were

those targets that normally receive input from CoCH-GFP⁺ RGCs, namely the vLGN (Fig. 5g-5i), the dLGN (Fig. 5j-5l), the OPN (Fig. 5m-5o) and the SC (Fig. 5v-5x). Thus, regeneration of CoCH-GFP⁺ RGC axons was target-specific. Moreover, the regenerated CoCH-GFP⁺ RGC axons avoided visual targets they normally fail to innervate: the SCN, the nucleus of the optic tract (NOT) and the MTN. Although these targets contained CTβ-594 labeled RGC axons (Fig. 5d, 5p, 5s), indicating they are capable of accepting regenerated RGC axons, none of the regenerated axons expressed GFP (Fig. 5e-5f, 5q-5r, 5t-5u), indicating they arise from other, non-CoCH-GFP⁺ RGC types.

To investigate whether other types of RGCs reconnect to appropriate targets, we examined regeneration in OPN4-GFP mice. OPN4 is expressed by a subpopulation of RGCs - so-called intrinsically-photosensitive RGCs (ipRGCs) - that are thought to be more amenable to regeneration²⁸. In normal unlesioned mice, the axons of OPN4-GFP⁺ RGCs heavily target the SCN, vLGN, IGL and OPN, while minimally targeting the dLGN and SC. OPN4-GFP⁺ RGC axons avoid the MTN entirely²⁸ (Supplementary Fig. 21). The biased-visual-stimulation/AAV2-cRheb1 protocol induced a subset of OPN4-GFP⁺ RGC axons to regenerate back to the brain where they reinnervated several correct targets such as the IGL (Supplementary Fig. 22j-22l) and avoided incorrect targets like the NOT and MTN (Supplementary Fig. 22p-22r).

In the brains of both CoCH-GFP mice and OPN4-GFP mice, we observed GFP⁺ axons that were not co-labeled with CTβ-594. To test the assumption that the GFP⁺/CTβ⁻ axons arise from the non-lesioned eye (Fig. 5i, 5l, 5o, 5x), we injected AAV2-cRheb1 into one eye of CoCH-GFP mice, nerve crushed the AAV2-cRheb1 eye, and then enucleated the opposite eye, forcing its RGC axons to degenerate. We then provided biased visual stimulation through the remaining eye every day for 3 weeks, in order to trigger regrowth of RGC axons (Fig. 6a-6c). In this experiment, any CTβ⁺/GFP⁺ axons observed in the brain must have originated from the lesioned eye. 6 of 9 mice in this group exhibited regenerated CoCH-GFP⁺ axons in the optic nerve and chiasm (Fig. 6d) as well as the vLGN (Fig. 6e-6g), dLGN (Fig. 6h-6j), and SC (Fig. 6k-6m) (Table 1) ('Group 10'). Importantly, all the regenerated CoCH-GFP⁺ axons were co-labeled with CTβ-594, indicating they regenerated from the lesioned eye. Together, our experiments on re-growth and steering of axons from GFP-labeled RGCs reveal the remarkable capacity of adult CNS axons to navigate back to and re-innervate their correct targets in the brain when provided with the appropriate combination of regeneration-inducing stimuli.

Functional restoration of visual behaviors

To test whether the regenerated RGC connections described above can support visual function, we assayed behavioral performance to four different tests of visual function²⁵. The optokinetic reflex probes the function of the AOS connections to the oculomotor brainstem²⁹, the pupillary light reflex (PLR) probes retino-pretectal connection to the OPN shell³⁰, the visual cliff test probes the retino-geniculo-cortical pathway³¹, and the looming avoidance response probes the retino-collicular pathway³²⁻³⁴. We tested three groups of mice: a pure-control 'non-lesioned' group, a unilaterally-optic-nerve-lesioned group that received no regeneration-enhancing treatment ('lesioned'/untreated), and a lesioned/treated

group (identical to 'Group 4' above), that received the biased-visual-stimulation/AAV2-cRheb1 treatments capable of inducing long-range axon regrowth into the brain (see methods) (Fig. 7a-7d). To ensure that any observed functional recovery was mediated by regenerated RGC connections originating from the lesioned eye and not by RGCs from the unlesioned eye, we sutured shut the unlesioned eye. The only exception to this was during testing of the consensual PLR where, by requirement, both eyes had to be kept open (see below).

First we assessed the optokinetic reflex (OKR) in which animals generate slip-compensating head movements in response to drifting-gratings moving along the horizontal axis (Fig. 7e). As described previously^{35,36} we quantified the percentage of 15-s trials in which the animals successfully tracked the stimulus (see methods). The non-lesioned group tracked ~33% of the stimulus trials ($n=5$ animals)- a value lower than is typical in binocularly sighted mice but still far greater than observed in the lesioned/untreated group which failed to track any stimulus trials ($n=5$ animals; 0% tracked) (Fig. 7f). The lesioned/treated mice, by contrast, tracked ~23% of the stimulus trials ($n=3$ animals), which was significantly more than the lesioned/untreated group and approached the percentage tracked by the non-lesioned group (Fig. 7f). This indicates that regenerated RGC axons can partially restore OKR behavior.

Next we measured the PLR, a behavior driven by ipRGC projections to the OPN shell^{30,37,38}. The PLR has both a 'direct' component and a 'consensual' component. The direct PLR represents constriction of the pupil in the *illuminated* eye. The consensual response is the constriction of the pupil in the *opposite* eye – mediated by intra-hemispheric connections (Supplementary Fig. 23). We recorded both the direct and consensual PLR to ipRGC-optimized blue light stimulation of the lesioned eye at 25 lux, for 30 sec^{30,38} (Fig. 7g-7h). Measuring the consensual PLR required opening the previously sutured eye at the time of testing. Both the direct and consensual response was dramatically reduced by ONC (Fig. 7i-7j). Restoration of the direct constriction response in the lesioned eye was increased compared to no treatment, but this was not statistically significant (Fig. 7i). There was no difference in direct (Fig. 7i) or consensual pupil constriction (Fig. 7j) between the treated and untreated groups, indicating that the regenerated RGC axons in the treated group failed to rescue the consensual pupil constriction.

Next, we performed the visual cliff test to assess depth perception and the functional integrity of the retino-geniculo-cortical pathway³¹. We placed each mouse on a platform, below which the floor on one side was painted with a low spatial frequency pattern of large black squares while the other was painted with a high spatial frequency pattern of small black squares. This creates an illusion of a shallow versus deep drop from the platform, respectively (Fig. 7k; see methods). Normal unlesioned mice chose to step down on the 'perceived shallow' side of the chamber in ~70% of trials, an effect that disappeared in mice with lesions to their optic nerves regardless of whether they received a treatment to induce regeneration or not (Fig. 7l). This indicates that the regeneration resulting from biased-visual-stimulation/AAV2-cRheb1 treatment failed to restore the connections that mediate visual cliff avoidance behavior. This could reflect defects in synapse formation and/or insufficient numbers of axons regenerating to the dLGN (discussed below).

Finally, we assayed the ‘visual fear’ response of animals to an overhead looming stimulus. In these experiments, animals are placed into a chamber equipped with a “hide” shelter and then a rapidly-expanding black circle is presented from the top of the chamber, a.k.a. ‘the looming stimulus’ (Fig. 7m; see methods)³². Upon presentation of the looming stimulus, normal mice either immediately froze or ran under the shelter (Fig. 7n)³². By contrast, none of the lesioned/untreated animals responded to the looming stimulus; they simply continued exploring the chamber (Fig. 7n). In the lesioned/treated group, 2 of 3 mice responded to the looming stimulus appropriately by running under the shelter to hide (Fig. 7n) and 1 of the lesioned/treated mice responded to looming stimulus by orienting its head and eyes upward each time the looming stimulus was presented, but never by freezing or hiding, indicating it perceived the stimulus, but failed to engage the appropriate behavioral response.

Overall, these results indicate that biased-visual-stimulation/cRheb1 treatments lead to regrowth of RGC axons that, in turn, can sustain partial recovery of some visual functions and vision-driven behaviors.

Discussion

By enhancing neural activity and mTOR signaling in RGCs, we observed long-distance, target-specific RGC axon regeneration in adult mice. These results indicate that, under the appropriate stimulus conditions, mature RGCs are capable of re-growing axons into the brain and forming connections with appropriate target neurons. This regeneration leads to partial recovery of several visual functions, suggesting that some degree of functional synapse re-formation likely can take place in the adult visual pathway.

Biased visual activity as a trigger for RGC axon growth

The greatest degree of regeneration was observed in mice that received enhanced RGC activity and unilateral lid suture (or eye removal) to eliminate vision through the unlesioned eye pathway. Why might this be so? Complete optic nerve lesions, as used here, eliminate the opportunity for binocular interactions among RGC axons located within central visual targets. Thus, the observed effects of unilateral visual bias may arise from one or several other sources. One possibility is that the bias effect is purely behavioral; that is, suturing shut the non-lesioned eye encouraged animals to keep the opposite, lesioned eye open, which in turn promoted more spiking activity in those RGCs. The reduced amount of regeneration observed in control animals where AAV2-cRheb1 and visual stimulation were provided through both eyes (as well as the controls that experienced no visual stimulation) support this idea. Another possibility is that, even though crushing the optic nerve triggers degeneration of RGC axons, their degeneration is not instantaneous but takes place 1-3 days following the crush. Thus, there may be a short window whereby binocular interactions driven by biased visual activity could boost or accelerate pathways controlling RGC regeneration in the open/lesioned eye. Regardless of the mechanism, the impact of biased visual stimulation on RGC axon regrowth is clearly evident from our data, because only in animals where one eye was sutured shut or removed did we observe long-distance regeneration of cRheb1-treated RGC axons from the non-sutured/intact eye.

In theory, visual stimulation could influence RGC axon regeneration by non-activity-dependent means, although the downstream mechanisms for that process are not clear at this time. However, our findings that a reduction in RGC activity via hM4Di/CNO prevents visual stimulation-mediated axon regeneration, and that increasing RGC activity with hM3Dq/CNO promotes axon regeneration, support the idea that RGC activity levels are a key parameter for regulating axon growth after injury. Increasing activity in ipRGCs has recently been shown to enhance RGC regrowth down the optic nerve but not regrowth into the brain³⁹ and electrical stimulation has been shown to prolong RGC survival *and* function in various models of ophthalmic diseases⁴⁰. Thus, there is growing evidence that electrical activity is a key parameter for adjusting the regrowth potential of CNS neurons.

Regrowth distance of RGC axons in various treatment paradigms

Our study demonstrates the remarkable capacity of adult CNS neurons to regenerate their axons long distances, provided they are treated with the appropriate growth-stimulating conditions. We found that enhanced RGC activity coupled with elevated mTOR signaling allowed axons to regenerate down the full length of the optic nerve and indeed, all the way into the brain. We note that other experiments that elevate mTOR signaling, such as deletion of the mTOR inhibitor PTEN, trigger a relatively greater number of RGC axons to regenerate than we observed here. One possible reason for this is that Cre-recombination is all-or-none whereas cRheb1 expression may vary somewhat between infected RGCs and thus, induce varying levels of p-S6 expression. However, we note that while PTEN deletion causes RGC axons to grow as far as the optic chiasm, it does not allow them to grow into the brain¹⁰ unless it is combined with one or more other treatments¹⁶ (Figs. 3-6). Together these data underscore the fact that multiple treatments applied in combination are needed to trigger regeneration of RGC axons back into the brain and they encourage additional exploration of the molecular pathways activated downstream of neural activity.

Specificity of axon regeneration in the mature CNS

By exploring genetically labeled RGC types- the alpha RGCs or ipRGCs- we found that RGCs have a remarkable capacity to reconnect to their correct targets in the brain while simultaneously avoiding incorrect targets. The fact that CoCH-GFP⁺ RGC axons are among the regenerating cohort is consistent with the previous work that identified cat alpha RGCs as the main group undergoing regeneration after sciatic nerve transplants⁴¹. These results are also in agreement with those of a recent study showing that alpha RGCs account for the majority of regenerating axons following PTEN deletion²⁷. We note that we observed many regenerated CT β ⁺ RGC axons, that were not GFP⁺ and that targeted brain areas not typically innervated by alpha RGCs (Figs. 4-6). This suggests that elevation of mTOR signaling with enhancement of RGC activity may recruit regeneration of not only alpha RGCs, but also other RGC types. The ability of OPN4-GFP⁺ axons to regenerate supports this idea and in the future it will be interesting to explore the regeneration capacity of other RGC types as well.

The fact that some RGCs are capable of re-innervating the correct brain targets is remarkable and, yet, this is not entirely surprising when one considers that others have observed target-specific re-innervation in other systems. Björklund and co-workers observed

that when the inhibitory effects of oligodendrocytes and myelin were neutralized, striatal and cortical projection neurons regenerated their axons long distances to re-innervate several of their correct targets in the substantia nigra, pontine nuclei, and cervical spinal cord⁴². More recently, Frank and co-workers observed that the central branch of lesioned dorsal root ganglion neurons undergo lamina-specific regeneration into the dorsal horn⁴³. Collectively, these studies suggest that in mammals, ligands and receptors that are expressed to ensure CNS axons arrive to and innervate their proper targets during development^{29,35}, may still be present, or even up-regulated, in response to RGC axon injury and/or regeneration in adulthood. Indeed, such up-regulation of guidance molecules in response to injury has been observed in the tectum/superior colliculus of cold-blooded vertebrates⁴⁴. It will be important to address this by exploring the molecular pathways that are activated in the RGC types that regenerate in our activity paradigm. In addition, it will be interesting to see if we can bias regrowth of different RGC types and evaluate their targeting by providing activity patterns tailored to their specific receptive field properties.

Functional and clinical implications

There are important functional implications of the anatomical regeneration we observed at the level of subcortically-mediated visual reflexes and behaviors. Combining elevation of mTOR signaling with enhancement of RGC activity via visual stimulation proved effective in partially restoring visual function in 2 out of the 4 visual assays we used. Curiously, the behaviors in which we observed recovery were those driven by the AOS (optokinetic reflex)^{29,35} and retino-SC connections (the looming avoidance response)³⁴ while the assays where we failed to observe any recovery were the pupil response (retino-OPN connection)³⁰ and visual cliff test. The first three behaviors involve retino-subcortical pathways and do not require the cortex²⁵ whereas the visual-cliff depth perception task is dependent on binocular vision and thus involves dLGN and V1³¹. The lack of recovery in the visual cliff task was somewhat surprising given that we observed regeneration of RGC axons to the dLGN- the nucleus that relays visual information to V1. The threshold for functional recovery of the retino-geniculo-cortical pathway may therefore be higher than that of the other retinofugal parallel pathways at the level of synapse formation and/or precision of within-target wiring. Indeed retinotopic and spatial precision of connections may not be a prerequisite for pathways driving OKR or looming since they involve large-field illumination, whereas visual cliff tasks require analysis of spatial frequency and thus, higher resolution image-formation.

Interestingly, we observed regeneration of RGC axons to the OPN- the nucleus that modulates pupillary light reflex- but we did not observe any substantial recovery of direct or consensual pupil constriction. It is, however, worth noting that we intentionally used low light intensities to stimulate the PLR so as not to allow spillover of light to the opposite, unlesioned eye. Although this was critical to avoid potential confounds, it is possible that higher light intensities could have driven functional activation of the PLR through the regenerated pathway connections. Regardless, our behavioral data support a model in which, restoration of neural pathways for visual function and perception may require a large number of RGCs to be recruited into the regeneration paradigm. In addition, a recent study probed the functional recovery of retinocollicular connections after distal nerve cut lesions

and found that anatomical regeneration occurred without functional restoration⁴⁵. Only by enhancing neural activity in regenerating RGCs did their axons recruit myelinating glia – just as RGCs do during development⁴⁶ - and allow for functional transmission between RGCs and their targets⁷⁵. Thus, additional sources of enhancing neural activity, in particular within the RGC populations that target the dLGN, may prove important for enhancing regeneration of mature central visual pathways and visual perception.

In conclusion, our findings demonstrating long-distance axon regeneration, specificity of connections and partial recovery of visual function may prove informative for devising treatments for the damaged visual system, spinal cord, or other CNS regions in human patients suffering from neurodegenerative diseases, or physical trauma.

Methods

Subjects

Mice of either sex ranging in age from postnatal day 30 to P80 were used, including 7 strains: wild-type mice with no GFP (C57BL/6) (from The Jackson Laboratory); Cochlin-EGFP mice (CoCH-GFP) (from MMRRC), Opsin 4 (melanopsin)-EGFP mice (OPN4-GFP) (from MMRRC), and PTEN^{fl/fl} mice, all of which were maintained on a C57/BL6 background. Mice were assigned to groups based on genotype (Figs. 5-6), or randomly selected for control or experimental groups (Figs. 1-4). Group sample sizes were chosen based upon previous studies^{10,14,18}. Animals were housed on a 12 h light/dark cycle and behavioral analyses were done at consistent afternoon hours during the light cycle. All experiments and procedures were done in accordance with approved animal protocols from APLAC and IACCUC committees at the University of California, San Diego.

Intra-vitreous injections of viruses and tracers

The following dyes and viruses were injected into the vitreal chamber of the eye using a Hamilton syringe as described previously²⁶: the anterograde tracer cholera toxin subunit beta (CT β) conjugated to Alexa Fluor 594 (CT β -594; Invitrogen) or to Alexa Fluor 488 (CT β -488; Invitrogen) to label RGC axons; adeno-associated virus serotype 2/1 with constitutively active Rheb1 (AAV2/1-cRheb1, 6×10^{10} ifu's/ml) to overexpress cRheb1; adeno-associated virus serotype 2 with hM4Di (rAAV2/hSyn-HA-hM4D(Gi)-IRES-mCitrine, 5.6×10^{12} vg/ml) and hM3Dq (rAAV2/hSyn-HA-hM3D(Gq)-IRES-mCitrine, 5.1×10^{12} vg/ml) (Gene Therapy Vector Core, UNC, NC) to overexpress hM4Di and hM3Dq, respectively; adeno-associated virus serotype 2 with Cre (AAV2-iCre, 1×10^{13} GC/ml) (Vector Biolabs) to knock out PTEN gene in PTEN^{fl/fl} mice or to use C57BL/6 mice for AAV control group after optic nerve crush. Injections were done using the following procedure: mice were anesthetized with inhalant isoflurane and a small hole was made near the ora serrata. The injection was made with a 33 gauge Hamilton needle and completeness of the eye fill was confirmed under a fluorescent dissecting microscope. CT β -injected animals were given a 2-day survival period to allow the tracer to travel down and label RGC axons and their terminals. After AAV2-cRheb1 or AAV2-hM4Di or AAV2-hM3Dq injections, we waited 2 weeks for the virus to express in the RGC population. All virus injections were performed with the experimenter blind to treatment conditions.

Intraperitoneal injection of rapamycin

Rapamycin (LC Laboratories; dissolved at 20 mg/ml in ethanol) was administered as described previously¹⁰. Before each administration, rapamycin was diluted in 5% Tween 80, 5% polyethylene glycol 400 (0.5–1.5 mg/ml). Rapamycin at 6 mg/kg or the vehicle (5% Tween 80, 5% polyethylene glycol 400 in PBS) was injected intraperitoneally after the AAV2-cRheb1 injection on the first day and then every 2 days for the duration of the experiment.

Intraperitoneal injection of clozapine-N-oxide

Clozapine-N-oxide (Tocris Bioscience; dissolved at 1mg/ml DMSO(0.5%)/saline) was administered as described previously²¹. CNO (1mg/kg for the hM3Dq group and 5mg/kg for the hM4Di group) was administered intraperitoneally twice each day for the duration of the experiment.

Optic nerve crush surgery

Animals were sedated by subcutaneous injection of ketamine/xylazine solution at 1µl/1g bodyweight. Jeweler's fine forceps (DUMONT #5, FST) were used to expose the optic nerve intraorbitally and crushed for 5 seconds at a distance approximately 2 mm from the posterior pole of the eye¹⁰. We carefully avoided damaging the ophthalmic artery and monitored the eye for any signs of bleeding in the period immediately after and for several hours and days following the crush. Ointment containing atropine sulphate (Bausch and Lomb, NDC 24208-825-55) was applied pre- and post-operatively to protect the cornea from drying. Any mice with vascular damage in the eye after optic nerve surgery were euthanized immediately after and were not included in the data set.

Visual stimulation

Mice were placed into a chamber surrounded by four 23" widescreen LCD monitors facing each other. The mice were exposed to high contrast (black/white): vertical lines drifting horizontally, 45 or 270 degree lines moving up and to the right or down and to the left, and horizontal lines moving vertically. The stimulus was delivered for 12-14 hours a day for the 21 days after optic nerve crush and was delivered during animals' wake time. Stimuli were powered by Optomotry VR 1.7.7 (CerebralMechanics Inc., Lethbridge, Alberta, Canada).

Eye-lid suture/ eye removal

After the animals were sedated, the margins of one eye-lid were trimmed slightly and the upper and lower lids were sutured together using nylon monofilament suture. To ensure that sutures remained intact, a drop of ophthalmic surgical bond was applied. To remove an eye, the animals were first sedated and using curved surgical scissors (ROBOZ, RS-5675) the eye was elevated slightly from the orbit and the optic nerve cut and eye removed. Afterward, the orbit was sutured shut.

Immunohistochemistry

After transcardial perfusion with saline (0.9% NaCl diluted in ddH₂O) followed by 4% paraformaldehyde (PFA), the eyes, optic nerves and brain were harvested and post-fixed in

4% PFA for 24 hours. The eyes were then transferred to phosphate buffered saline (PBS) and the optic nerve and brain placed in 30% sucrose for cryoprotection. The optic nerve was sectioned using a sledge microtome, cutting longitudinally at 15 μm . The brain was sectioned coronally at 30 μm . All tissue sections were included for analysis. Retinas, optic nerves, and brain tissue were kept at 4° Celsius overnight using the following antibodies: rabbit-anti-RBPMS (PhosphoSolutions, 1:1000), to label RGCs; rabbit- or guinea pig-anti-GFP (SySy; 1:1000), to enhance GFP signal; rabbit-anti-p-S6 (Cell Signaling Technology; 1:250), to label phosphorylated S6 protein; mouse anti-SMI-32 (Sternberger monoclonals, 1:2000) to label alpha and other large soma RGC types; rabbit anti-melanopsin (Advanced Targeting Systems, 1:1000). For secondary detection, Alexa Fluor 488 goat anti-rabbit or anti-guinea pig (1:1000; Life Technologies), or Alexa Fluor 594 goat anti-rabbit (1:1000; Life Technologies) were used. Immunostained tissues were imaged with with an epifluorescence microscope (Zeiss Axio imager 2 with HR Zeiss camera, 10X and 20X objectives).

Cell number quantification

We compared p-S6 expression (cell numbers) in the retinas of AAV2-cRheb1 injected animals and animals control injected with saline. After we immunostained the retinas with identical protocols for the downstream marker of phosphorylated mTOR, p-S6, each flat mount retina was imaged with an epifluorescence microscope. Multiple 500 μm \times 500 μm regions of the retina were analyzed for each animal ($n = 5$ mice per group). Photoshop (Adobe, CS6) was used to convert each image to gray scale and to threshold the image to eliminate background noise (same thresholds applied). Each p-S6⁺ profile was then counted and included in the analysis. Using the same analysis, we also quantified the number of RGCs in different experimental conditions by immunostaining the retinas for the RGC marker, RBPMS²².

Axon quantification in the optic nerve

After we imaged the serial optic nerve sections, Photoshop (Adobe, CS6) was used to stitch the images into a complete montage. Lines spaced equidistant from each other at 500 μm intervals from the rear of the eye to the optic chiasm were introduced to the montage for “bin-by-bin” axon quantification. We manually counted the number of individual axons that transected each vertical line. As used by other groups^{10,16}, we quantified the total number of regenerating axons, Σ_{ad} , by using the following formula: $\Sigma_{ad} = \pi r^2 \times [\text{average axons/mm}]/t$, where total number of axons extending the distance d in a nerve having a radius of r , was estimated by summing overall sections with thickness t (in our case, 15 μm). The axon counts were verified by a blind-to-condition, independent viewer.

Electrophysiology

Procedures were similar to those described previously³⁵. Briefly, retinas were harvested and dissected in gassed (95% O₂ and 5% CO₂) Ames medium (Sigma) under infrared illumination, and cut along the dorsal-ventral axis. Only ventral pieces were used. A piece of retina was placed in a chamber on an upright microscope and superfused (~5ml/min) with gassed Ames medium heated to 33-35 °C. RGCs expressing mCitrine were visualized at 40X by attenuated mercury light passed through a GFP dichroic mirror, and then targeted for

recording under IR illumination. Cells were recorded with borosilicate glass pipettes (4-6 M Ω) filled with intracellular solution containing (in mM): 120 K-methanesulphonate 10 HEPES, 5 NaCl, 0.1 EGTA, 2 ATP-Mg²⁺, and 0.3 GTP-Na, titrated to pH 7.3. Chemicals were purchased from Sigma-Aldrich or Tocris.

Current-evoked spiking responses were recorded in response to a series of 10 monotonically increasing 20 pA current steps. The baseline current step used for analysis varied between cells (20-80 pA) but was always the smallest step that produced at least one spike under control conditions. Patterned light stimuli were generated by custom software developed in Psychophysics Toolbox and MATLAB. Stimuli were projected onto the retina using a Dell video projector (M109s DLP) custom fitted with a UV LED (NC4U134A; final emission, 398nm; Nichia), attenuated by a neutral density 1.0 filter, and focused using a 10X objective to the level of rod and cone outer segments. Stimulus intensity produced 2.6×10^5 R*/S-cone/sec. Stable S-cone mediated responses can be recorded from RGCs in the ventral mouse retina following targeting by epifluorescence under these conditions. The receptive field center was mapped by recording responses to square-wave modulations of a 300 μ m diameter spot at eight positions. In subsequent experiments, stimuli were presented as a contrast pulse (100% Weber contrast), 200-400 microns in diameter. The same size stimulus was always used for both control and CNO recordings for a given cell.

Behavioral analyses

Optokinetic reflex—Mice were placed on an elevated platform surrounded by four 23' widescreen LCD monitors. Each trial consisted of vertical drifting-bar stimuli presented at a spatial frequency of 0.16 cycles/degree and temporal frequency of 12 degrees/s- the optimal stimulus for driving the OKR^{35,36}. Each trial lasted 15 s; if the head of the mouse moved in concert with the gratings, the trial was scored as “tracked.” Each mouse was presented with 10 trials per day, for 3 consecutive days, at the same time of day. Responses were averaged to generate a mean percentage of trials tracked ($n = 3-5$ mice per group; see text).

Pupillary light reflex—Mice were dark-adapted within their home cage for one hour prior to the experiment. All mice were unanesthetized and restrained by hand for the duration of the experiment. A single blue (470 nm) LED was placed in front of the stimulated eye. Both the direct (stimulated eye) and consensual (contralateral eye) PLR were recorded with two infrared video cameras placed on either side of the head. The pupils were recorded before (baseline) and during (constriction) the light stimulus (30 s at 25 lux). The light intensity was reduced to 25 lux to prevent light spill over to the other eye. Individual frames of the initial resting pupil size (baseline) and at maximal constriction were extracted from the video recordings and pupil diameters were measured using ImageJ. The percentage of the pupil constriction^{30,38} was calculated from the pupil diameter measurements at the initial resting size and maximal constriction. ($n = 3-5$ mice per group; see text).

Visual cliff—The visual cliff behavior was analyzed in an open-top plexiglass chamber. Half of the box protruded from the counter to provide 3 ft depth. The box on the counter displayed a base with a checkerboard pattern and the box off the counter showed the base with the same checkerboard pattern, except for the 3 ft of depth. A 2' high platform was

stationed in the middle of the box intersecting both the shallow side and deep side. The mouse is placed on top of the platform and can choose between the two sides. If the mouse stepped down to the shallow side, that trial was scored as “relative depth perceived.” If the mouse either stepped down to the deep side or stayed on top of the platform for 5 minutes, that trial was scored as “relative depth not perceived.” Each mouse performed this task 5 times per day for 3 days. The visual cliff behavior was averaged to generate mean percentage of trials in which the mouse chose to step down to the “shallow” side ($n = 3-5$ mice per group; see text).

Looming response behavior analysis—The looming response is a well documented behavior in which mice freeze or flee to an escape area or “hide” in response to an overhead dark expanding disk^{32,34}. This analysis was performed with mice in an open-top plexiglass chamber. A 24" LCD monitor was stationed on top of the chamber facing downward to display the stimulus. One end of the box included a black shelving board to provide a “hide” shelter. A video camera recorded the mouse’s movements during the trial at 30 fps. The mouse was free to roam inside the box for 5 min before the first presentation of the stimulus. The looming stimulus was presented 3 times during a 3-second epoch. If the mouse responded to the stimulus by either freezing, or hiding in the shelter, that trial was scored as “looming response.” Each animal performed the task once. The percentage of looming responses/total looming stimulus presentations were averaged for each animal as to generate a mean percentage of trials responded ($n = 3-5$ mice per group; see text).

Statistics

Statistical tests indicated in our study were performed using Prism 7 (GraphPad Software, La Jolla, CA). In addressing our hypothesis that visual stimulation alone or together with cRheb1 overexpression and/or other manipulations can enhance axon regeneration, we tested the increases in RGC axon regeneration by one-tailed *t*-test. Continuous data was tested with parametric tests and data was assumed to be normally distributed, but this was not formally tested.

Supplementary Material

Refer to Web version on PubMed Central for supplementary material.

Acknowledgments

The authors would like to thank Drs. T. Seabrook, O. Dhande, R. El-Danaf, and other members of the Huberman lab for helpful comments on earlier versions of this manuscript. This work was supported by grants from the National Institutes of Health National Eye Institute R01, NIH/NEI R01EY026100 (ADH), The Pew Biomedical Foundation, The McKnight Foundation, and The Glaucoma Research Foundation Catalyst for a Cure Initiative.

References

1. Liu K, Tedeschi A, Park KK, He Z. Neuronal intrinsic mechanisms of axon regeneration. *Annu Rev Neurosci.* 2011; 34:131–152. [PubMed: 21438684]
2. Vidal-Sanz M, Bray GM, Villegas-Perez MP, Thanos S, Aguayo AJ. Axonal regeneration and synapse formation in the superior colliculus by retinal ganglion cells in the adult rat. *J Neurosci.* 1987; 7:2894–2907. [PubMed: 3625278]

3. Chen MS, et al. Nogo-A is a myelin-associated neurite outgrowth inhibitor and an antigen for monoclonal antibody IN-1. *Nature*. 2000; 403:434–439. [PubMed: 10667796]
4. Cafferty WB, Duffy P, Huebner E, Strittmatter SM. MAG and OMgp synergize with Nogo-A to restrict axonal growth and neurological recovery after spinal cord trauma. *J Neurosci*. 2010; 30:6825–6837. [PubMed: 20484625]
5. Davies SJ, et al. Regeneration of adult axons in white matter tracts of the central nervous system. *Nature*. 1997; 390:680–683. [PubMed: 9414159]
6. Gallo V, Bertolotto A, Levi G. The proteoglycan chondroitin sulfate is present in a subpopulation of cultured astrocytes and in their precursors. *Dev Biol*. 1987; 123:282–285. [PubMed: 3114027]
7. Bundesen LQ, Scheel TA, Bregman BS, Kromer LF. Ephrin-B2 and EphB2 regulation of astrocyte-meningeal fibroblast interactions in response to spinal cord lesions in adult rats. *J Neurosci*. 2003; 23:7789–7800. [PubMed: 12944508]
8. Pasterkamp RJ, Giger RJ, Verhaagen J. Regulation of semaphorin III/collapsin-1 gene expression during peripheral nerve regeneration. *Exp Neurol*. 1998; 153:313–327.
9. Shewan D, Berry M, Cohen J. Extensive regeneration in vitro by early embryonic neurons on immature and adult CNS tissue. *J Neurosci*. 1995; 15:2057–2062. [PubMed: 7891152]
10. Park KK, et al. Promoting axon regeneration in the adult CNS by modulation of the PTEN/mTOR pathway. *Science*. 2008; 322:963–966. [PubMed: 18988856]
11. Meyer-Franke A, et al. Depolarization and cAMP elevation rapidly recruit TrkB to the plasma membrane of CNS neurons. *Neuron*. 1998; 21:681–693. [PubMed: 9808456]
12. Leaver SG, et al. AAV-mediated expression of CNTF promotes long-term survival and regeneration of adult rat retinal ganglion cells. *Gene Ther*. 2006; 13:1328–1341. [PubMed: 16708079]
13. Moore DL, et al. KLF family members regulate intrinsic axon regeneration ability. *Science*. 2009; 326:298–301. [PubMed: 19815778]
14. Smith PD, et al. SOCS3 deletion promotes optic nerve regeneration in vivo. *Neuron*. 2009; 64:617–623. [PubMed: 20005819]
15. Pernet V, Schwab ME. Lost in the jungle: new hurdles for optic nerve axon regeneration. *Trends in Neurosci*. 2014; 37:381–387.
16. de Lima S, et al. Full-length axon regeneration in the adult mouse optic nerve and partial recovery of simple visual behaviors. *Proc Natl Acad Sci U S A*. 2012; 109:9149–9154. [PubMed: 22615390]
17. Chierzi S, Strettoi E, Cenni MC, Maffei L. Optic nerve crush: axonal responses in wild-type and bcl-2 transgenic mice. *J Neurosci*. 1999; 19:8367–8376. [PubMed: 10493738]
18. Sun F, et al. Sustained axon regeneration induced by co-deletion of PTEN and SOCS3. *Nature*. 2011; 480:372–376. [PubMed: 22056987]
19. Luo X, et al. Three-dimensional evaluation of retinal ganglion cell axon regeneration and pathfinding in whole mouse tissue after injury. *Exp Neurol*. 2013; 247:653–662. [PubMed: 23510761]
20. Goldberg JL, et al. Retinal ganglion cells do not extend axons by default: promotion by neurotrophic signaling and electrical activity. *Neuron*. 2002; 33:689–702. [PubMed: 11879647]
21. Urban DJ, Roth BL. DREADDs (Designer Receptors Exclusively Activated by Designer Drugs): chemogenetic tools with therapeutic utility. *Annu Rev Pharmacol Toxicol*. 2015; 55:399–417. [PubMed: 25292433]
22. Kwong JM, Caprioli J, Piri N. RNA binding protein with multiple splicing: a new marker for retinal ganglion cells. *Invest Ophthalmol Vis Sci*. 2010; 51:1052–1058. [PubMed: 19737887]
23. Yamagata K, et al. rheb, a growth factor- and synaptic activity-regulated gene, encodes a novel Ras-related protein. *J Biol Chem*. 1994; 269:16333–16339. [PubMed: 8206940]
24. Maier IC, et al. Constraint-induced movement therapy in the adult rat after unilateral corticospinal tract injury. *J Neurosci*. 2008; 28:9386–9403. [PubMed: 18799672]
25. Dhande OS, Stafford BK, Lim JA, Huberman AD. Contributions of retinal ganglion cells to subcortical visual processing and behaviors. *Ann Rev Vis Sci*. 2015; 1:291–328. [PubMed: 28532372]

26. Huberman AD, et al. Architecture and activity-mediated refinement of axonal projections from a mosaic of genetically identified retinal ganglion cells. *Neuron*. 2008; 59:425–438. [PubMed: 18701068]
27. Duan X, et al. Subtype-specific regeneration of retinal ganglion cells following axotomy: effects of osteopontin and mTOR signaling. *Neuron*. 2015; 85:1244–1256. [PubMed: 25754821]
28. Hattar S, Liao HW, Takao M, Berson DM, Yau KW. Melanopsin-containing retinal ganglion cells: architecture, projections, and intrinsic photosensitivity. *Science*. 2002; 295:1065–1070. [PubMed: 11834834]
29. Sun LO, et al. Functional assembly of accessory optic system circuitry critical for compensatory eye movements. *Neuron*. 2015; 86:971–984. [PubMed: 25959730]
30. Güler AD, et al. Melanopsin cells are the principal conduits for rod-cone input to non-image-forming vision. *Nature*. 2008; 453:102–105. [PubMed: 18432195]
31. Leamey CA, et al. Ten_m3 regulates eye-specific patterning in the mammalian visual pathway and is required for binocular vision. *PLoS Biol*. 2007; 9
32. Yilmaz M, Meister M. Rapid innate defensive responses of mice to looming visual stimuli. *Current Biology*. 2013; 23:2011–2015. [PubMed: 24120636]
33. Shang C, et al. A parvalbumin-positive excitatory visual pathway to trigger fear responses in mice. *Science*. 2015; 348:1472–1477. [PubMed: 26113723]
34. Zhao X, Liu M, Cang J. Visual cortex modulates the magnitude but not the selectivity of looming-evoked responses in the superior colliculus of awake mice. *Neuron*. 2014; 84:202–213. [PubMed: 25220812]
35. Osterhout JA, Stafford BK, Nguyen PL, Yoshihara Y, Huberman AD. Contactin-4 mediates axon-target specificity and functional development of the accessory optic system. *Neuron*. 2015; 86:985–999. [PubMed: 25959733]
36. Prusky GT, Silver BD, Tschetter WW, Alam NM, Douglas RM. Experience-dependent plasticity from eye opening enables lasting, visual cortex-dependent enhancement of motion vision. *J Neurosci*. 2008; 28:9817–9827. [PubMed: 18815266]
37. Lucas RJ, Douglass RH, Foster RG. Characterization of an ocular photopigment capable of driving pupillary constriction in mice. *Nat Neurosci*. 2001; 4:621–626. [PubMed: 11369943]
38. Sweeney NT, Tierney H, Feldheim DA. Tbr2 is required to generate a neural circuit mediating the pupillary light reflex. *J Neurosci*. 2014; 34:5447–5453. [PubMed: 24741035]
39. Li S, et al. Promoting axon regeneration in the adult CNS by modulation of the melanopsin/GPCR signaling. *Proc Natl Acad Sci U S A*. 2016; 113:1937–1942. [PubMed: 26831088]
40. Fu L, Lo AC, Lai JS, Shih KC. The role of electrical stimulation therapy in ophthalmic diseases. *Graefes Arch Clin Exp Ophthalmol*. 2015; 253:171–176. [PubMed: 25501299]
41. Watanabe M, Sawai H, Fukuda Y. Number, distribution, and morphology of retinal ganglion cells with axons regenerated into peripheral nerve graft in adult cats. *J Neurosci*. 1993; 13:2015–2017.
42. Victorin K, Brundin P, Gustavli B, Lindvall O, Björklund A. Reformation of long axon pathways in adult rat central nervous system by human forebrain neuroblasts. *Nature*. 1990; 347:556–558. [PubMed: 1699131]
43. Harvey P, Gong B, Rossomando AJ, Frank E. Topographically specific regeneration of sensory axons in the spinal cord. *Proc Natl Acad Sci U S A*. 2010; 107:11585–11590. [PubMed: 20534446]
44. King CE, et al. Transient up-regulation of retinal EphA3 and EphA5, but not ephrin-A2, coincides with re-establishment of a topographic map during optic nerve regeneration in goldfish. *Exp Neurol*. 2003; 182:593–599.
45. Bei F, et al. Restoration of visual function by enhancing conduction in regenerated axons. *Cell*. 2016; 164:219–232. [PubMed: 26771493]
46. Barres BA, Raff MC. Axonal control of oligodendrocyte development. *J Cell Biol*. 1999; 147:1123–1128. [PubMed: 10601327]

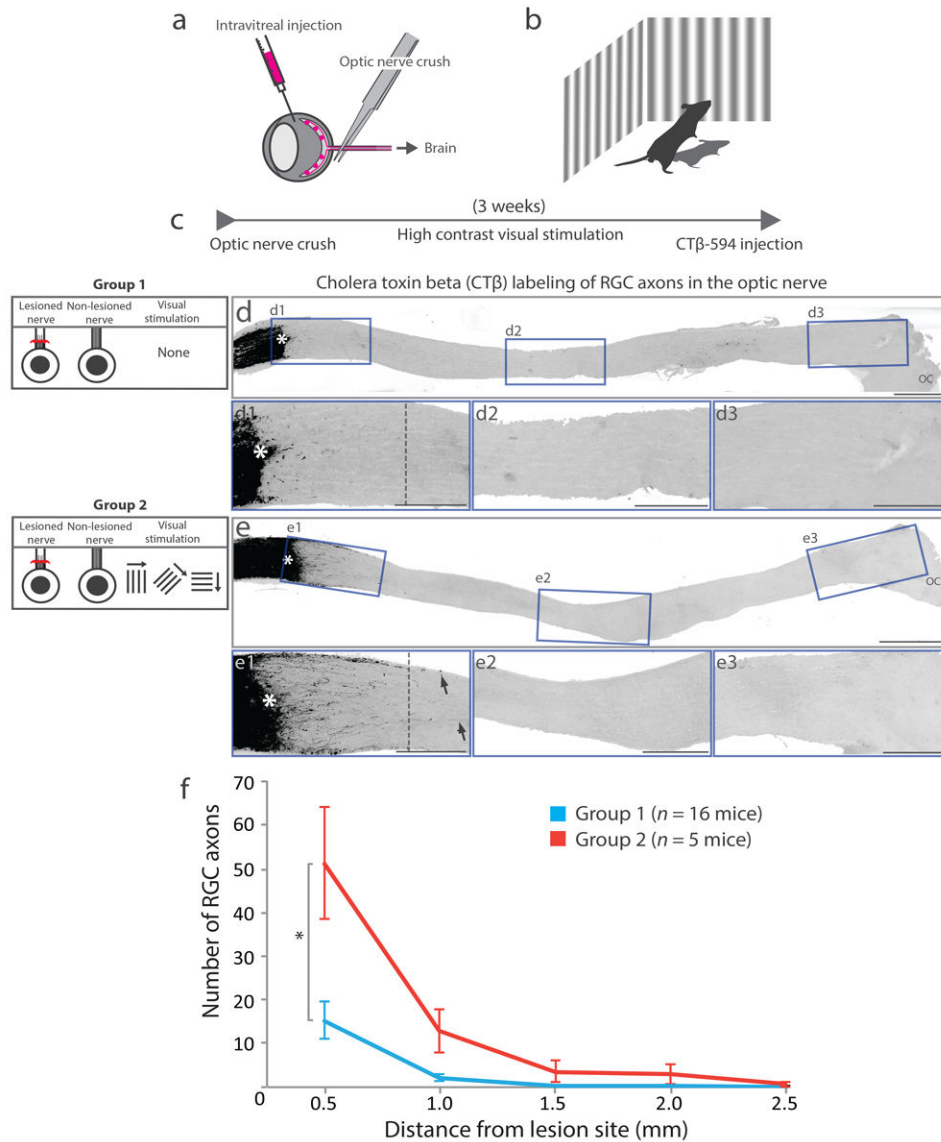


Figure 1. Visual stimulation triggers regeneration of RGC axons

(a) Experimental design of intravitreal injection and optic nerve crush. (b) Schematic diagram of high contrast visual stimulation. (c) Experimental timeline. (d-e) Low magnification images of CTβ-labeled optic nerves from the control group ('Group 1,' $n = 16$ mice) (d) and visual stimulation group ('Group 2,' $n = 5$ mice) (e). (d1-d3) High magnification images from insets in (d). (e1-e3) High magnification images from insets in (e). Arrows in (e1) point to regenerating axons. Asterisk in (d), (d1), (e), and (e1) is the lesion site. Vertical dashed line in (d1) and (e1) indicates 500 μm mark beyond the lesion site for axon quantification. (f) Line graph showing the number of regenerating axons as a function of distance from the lesion site (data presented as mean \pm SEM). Asterisks indicate significance in unpaired one-tailed Student's t -test; $*P < 0.05$ ($p = 0.032$, $t = 2.393$, $dF = 4.83$; $p = 0.0658$, $t = 1.873$, $dF = 4.167$; $p = 0.1465$, $t = 1.208$, $dF = 4.048$; $p = 0.1793$, $t = 1.035$, $dF = 4.027$; $p = 0.213$, $t = 0.8829$, $dF = 4.1$). Scale bar in (d-f) = 500 μm ; (d1-d3),

(e1-e3) = 250 μ m. OC in panels (d) and (e) denotes optic chiasm. Note: The ‘Group 1’ includes control animals that received intravitreal injections of either AAV2-Cre ($n = 5$ mice) or saline vehicle ($n = 6$ mice) or control animals that received no injections ($n = 5$ mice) before the optic nerve crush. We observed no significant difference in the number of RGC axons past the lesions among the three control groups (Supplementary Fig. 1).

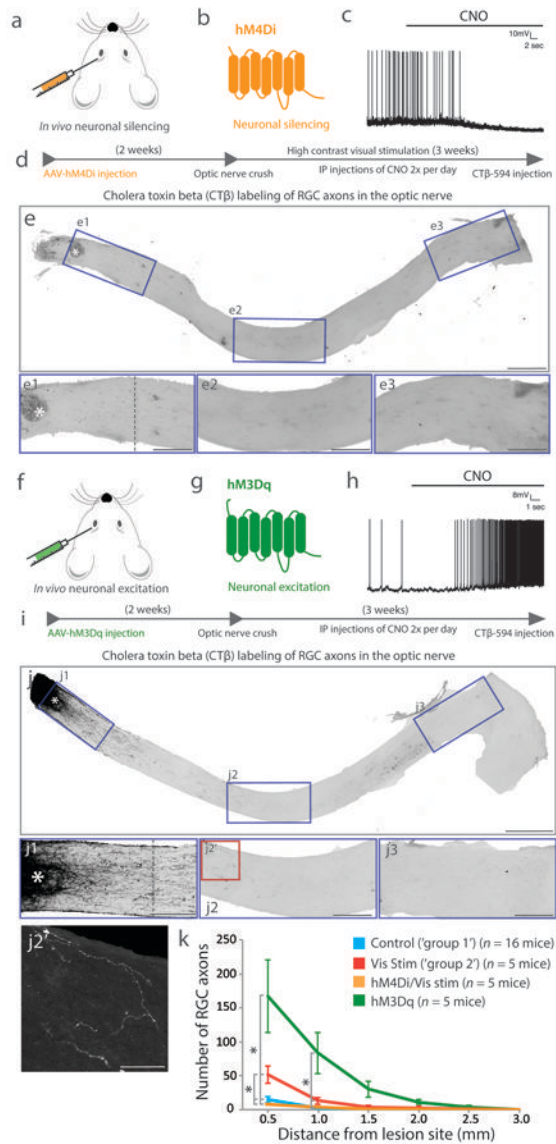


Figure 2. Neural activity regulates regeneration of RGC axons

(a) Schematic diagram of intravitreal injections. (b) Schematic diagram of hM4Di receptor. (c) Representative example of spike train before and after CNO administration during whole cell recording of a RGC infected with AAV2-hM4Di-mCitrine. (d) Experimental timeline. (e) Low magnification images of CT β -labeled optic nerves from the AAV2-hM4Di group ($n = 5$ mice). (e1-e3) High magnification images from insets in (e). (f) Schematic diagram of intravitreal injection. (g) Schematic diagram of hM3Dq receptor. (h) Representative example of spike train before and after CNO administration during whole cell recording of a RGC infected with AAV-hM3Dq-mCitrine. (i) Experimental timeline. (j) Low magnification images of CT β -labeled optic nerves from the AAV2-hM3Dq group ($n = 5$ mice). (j1-j3) High magnification images from insets in (j). (j2^{*}) Higher magnification image from inset in (j2). Asterisk in (f), (f1), (j), and (j1) is the lesion site. Vertical dashed line in (f1) and (h1) indicates 500 μ m mark beyond the lesion site for axon quantification. (k) Line graph

showing the number of regenerating axons as a function of distance from the lesion site (data presented as mean \pm SEM). Asterisks indicate significance in unpaired one-tailed Student's *t*-test; * $P < 0.05$ (statistics results in the Supplementary Table 1). Scale bar in (e) and (j) = 500 μm ; (e1-e3), (j1-j3) = 250 μm ; (j2') = 50 μm .

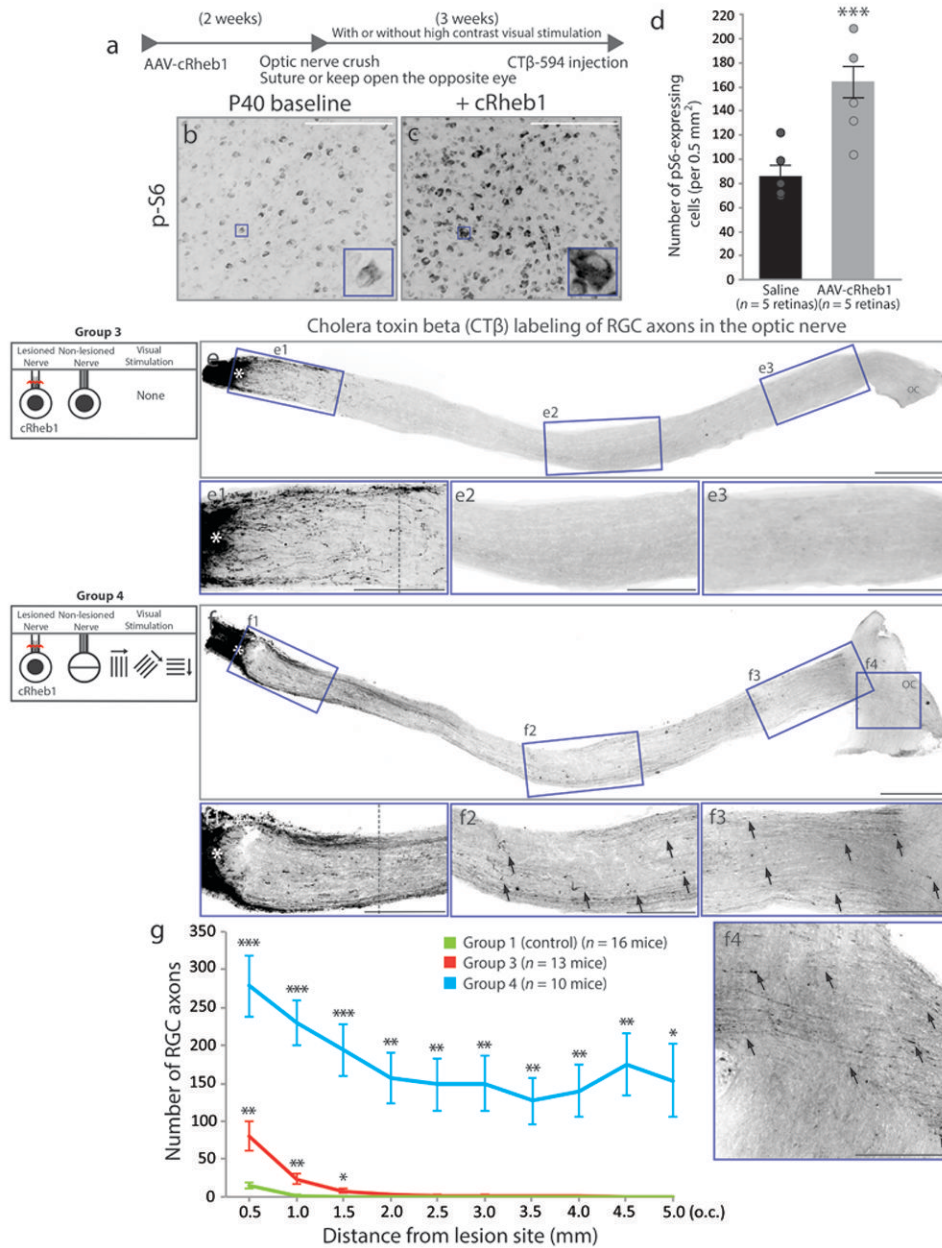


Figure 3. Combining biased visual stimulation and enhancement of mTOR signaling with cRheb1 overexpression triggers long distance regeneration of RGC axons

(a) Experimental time line. (b) and (c) Images of flat mount retina immunostained with p-S6 for baseline levels (b) and cRheb1-induced levels of p-S6 expression (c) with a high magnification image of inset. (d) Quantification of p-S6-expressing cells ($n = 5$ retinas per group) (data presented as mean \pm SEM). Asterisks indicate statistical significance in unpaired one-tailed Student's t -test; $***P < 0.0005$ ($p = 0.0003$, $t = 1.553$, $dF = 19.67$). (e-f), Low magnification image of CT β -labeled optic nerve in AAV2-cRheb1 group ('Group 3,' $n = 13$ mice) (e) and AAV2-cRheb1 plus biased visual stimulation group ('Group 4,' $n = 10$ mice) (f). (e1-e3), High magnification images from insets in (e). (f1-f4) High magnification images from insets in (f). Arrows in (f2), (f3), and (f4) point to regenerating fibers. Asterisk

in **(e)**, **(e1)**, **(f)**, and **(f1)** shows the lesion site. Vertical dashed line in **(e1)** and **(f1)** indicates 500 μm mark beyond the lesion site for axon quantification. **(g)** Line graph showing the number of regenerating axons as a function of distance from the lesion site (data presented as mean \pm SEM). Asterisks indicate statistical significance in unpaired one-tailed Student's *t*-test; * $P < 0.05$; ** $P < 0.005$; *** $P < 0.0005$ (statistics results in the Supplementary Table 2). Scale bar in **(c)** = 250 μm ; **(e)** and **(f)** = 500 μm ; **(e1-e3)** and **(f1-f4)** = 250 μm .

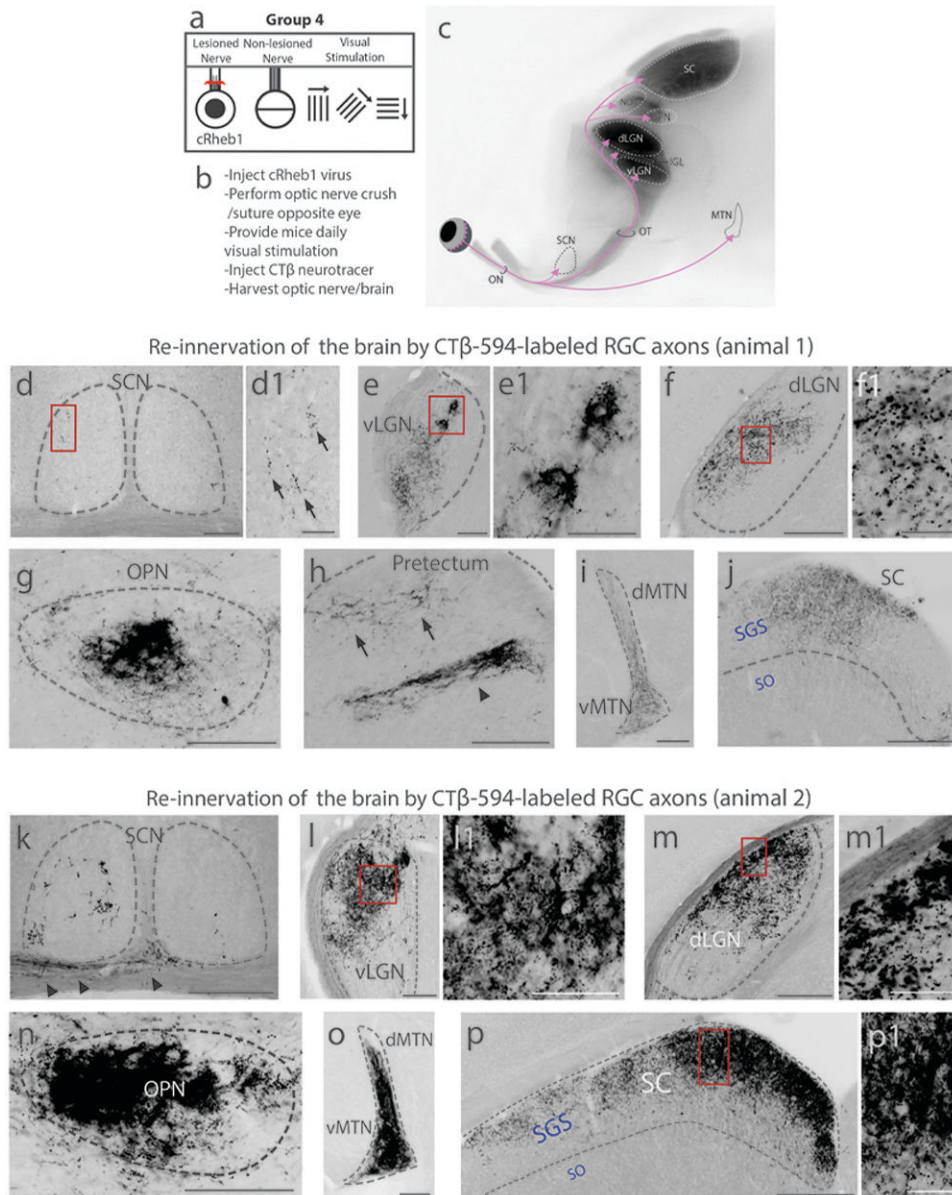


Figure 4. Combining biased visual stimulation and enhancement of mTOR signaling with cRheb1 overexpression allows RGCs to regenerate their axons back to their targets
(a) Schematic of experimental group ('Group 4'). **(b)** Summary of the experiments for the combined treatments. **(c)** Schematic of a sagittal mouse brain section showing the major visual targets labeled with CT β . **(d-j)** Coronal brain sections from one animal showing CT β -labeled regenerating RGC axons in the suprachiasmatic nucleus (SCN) (**d** and **d1**), ventral lateral geniculate nucleus (vLGN) (**e** and **e1**), dorsal lateral geniculate nucleus (dLGN) (**f** and **f1**), olivary pretectal nucleus (OPN) (**g**), pretectum (**h**), medial terminal nucleus (MTN; d, dorsal; v, ventral) (**i**), and superior colliculus (SC; SGS, stratum griseum superficiale; SO, stratum opticum) (**j**). Dashed lines in **(d-j)** indicate the boundary of each visual target. Arrows in **(d1)** point to regenerating axons within the SCN and arrows in **(h)** point to regenerating axons in pretectum. Arrowhead in **(h)** indicates highly specific axon

regeneration of posterior limitans. **(k-p)** Coronal sections of another animal's brain, showing CT β -labeled regenerating RGC axons in SCN (**k**), vLGN (**l** and **l1**), dLGN (**m** and **m1**), OPN (**n**), MTN (**o**), and SC (**p** and **p1**). **(p1)** SGS: stratum griseum superficiale; SO: stratum opticum. Dotted outlines in **(k-p)** indicate the approximate area of each visual target.

Arrowheads in **(k)** show axons in optic chiasm that do not re-innervate to visual targets.

Scale bar in **(d)** = 100 μ m; **(d1)** = 20 μ m; **(e)** = 100 μ m; **(e1)** = 50 μ m; **(f)** = 200 μ m; **(f1)** = 50 μ m; **(g)** = 100 μ m; **(h)** = 50 μ m; **(i)** = 100 μ m; **(j)** = 200 μ m; **(k)** = 200 μ m; **(l)** = 100 μ m; **(l1)** = 50 μ m; **(m)** = 200 μ m; **(m1)** = 100 μ m; **(n)** = 100 μ m; **(o)** = 100 μ m; **(p)** = 250 μ m; and **(p1)** = 50 μ m.

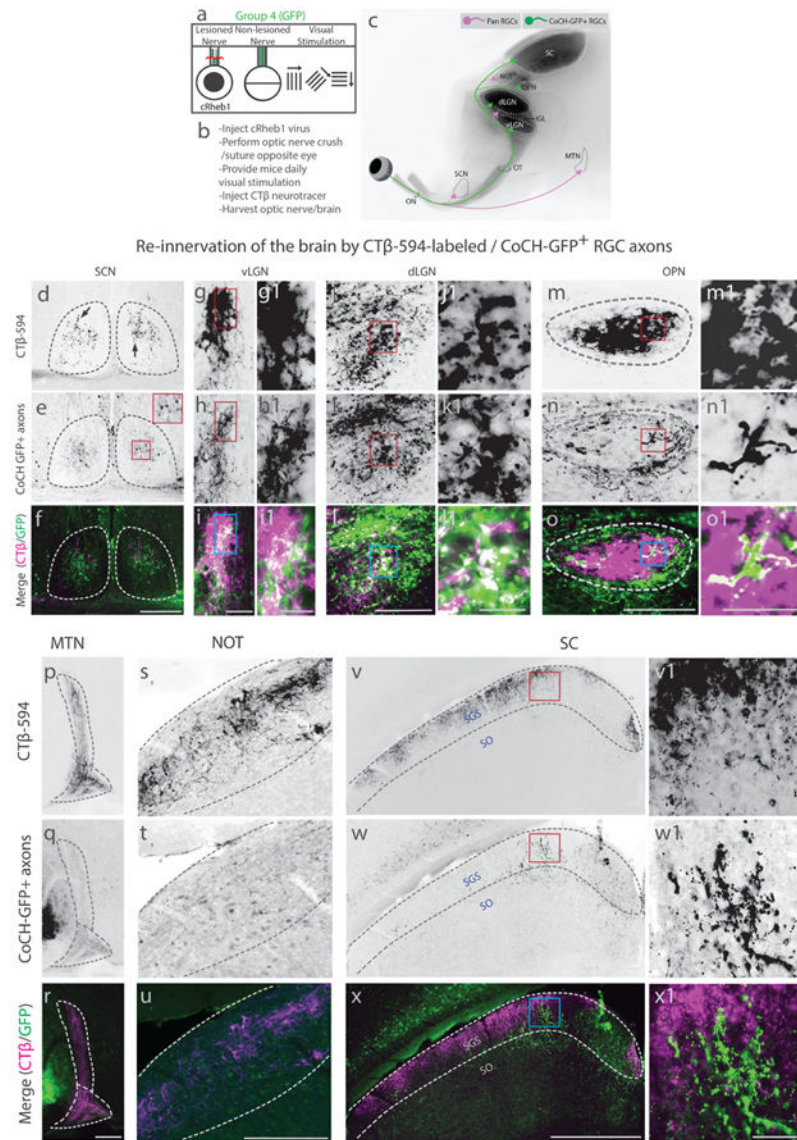


Figure 5. Specificity of axon regeneration from distinct RGC types to their visual targets
(a) Schematic of experimental group ('Group 4'). **(b)** Summary of the experiments for the combined treatments. **(c)** Schematic of sagittal mouse brain with retinofugal projections from CoCH GFP⁺ RGCs shown in green, and pan RGCs shown in magenta. **(d-x)** Images of CTβ-labeled regenerated axons, GFP-immunostained coronal sections of brain from CoCH GFP animal showing RGC axons in the SCN (**d-f**), vLGN (**g-i**; insets **g1-i1**), dLGN (**j-l**; insets **j1-l1**), OPN (**m-o**; insets **m1-o1**), MTN (**p-r**), NOT (**s-u**), and SC (**v-x**; insets **v1-x1**). Dashed outline in (**d-x**) indicates the approximate boundary of each visual target. Scale bar in (**d-f**) = 200 μm; (**g-i**) = 50 μm; (**g1-i1**) = 25 μm; (**j-l**) = 100 μm; (**j1-l1**) = 25 μm; (**m-o**) = 100 μm; (**m1-o1**) = 25 μm; (**p-r**) = 100 μm; (**s-u**) = 250 μm; (**v-x**) = 500 μm; (**v1-x1**) = 50 μm.

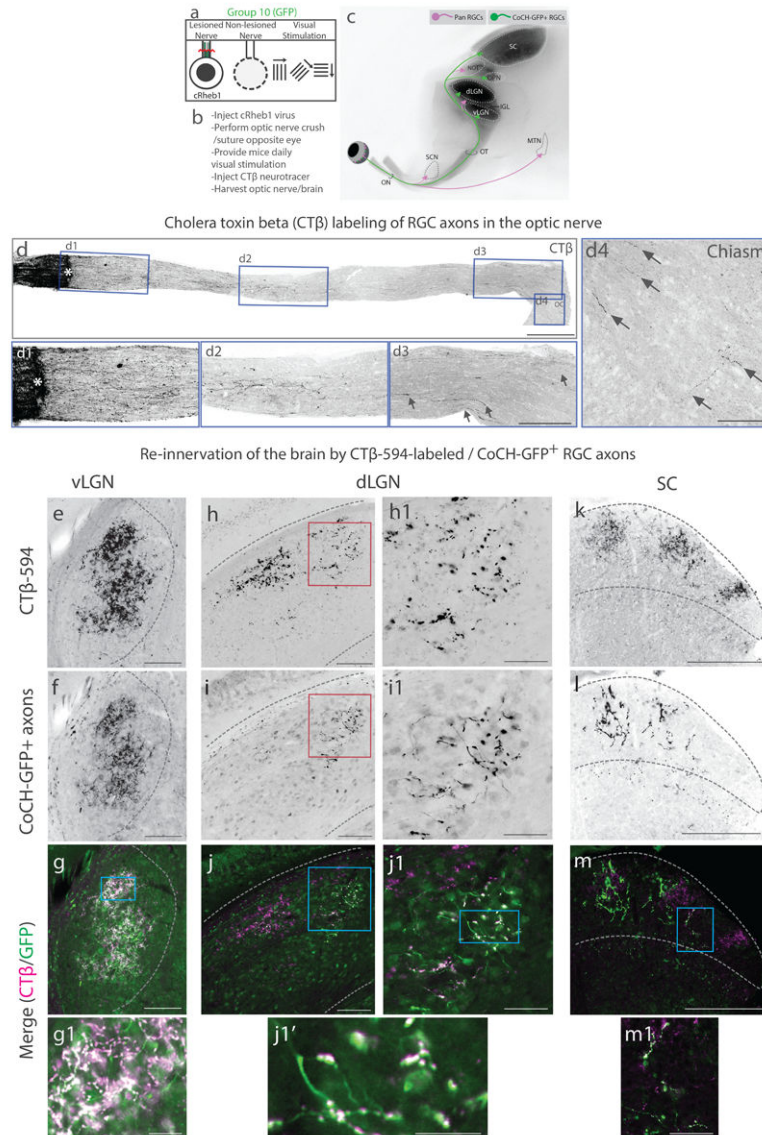


Figure 6. Removing one eye and enhancement of mTOR signaling with cRheb1 overexpression trigger RGC regeneration to correct visual targets in the brain
(a) Schematic of the experimental group ('Group 10,' $n = 9$ mice). **(b)** Summary of the experiments for the combined treatments. **(c)** Schematic of sagittal mouse brain with projections from CoCH GFP⁺ RGCs in green and pan RGCs shown in magenta. **(d)** Low magnification image of CT β -labeling of regenerated RGC axons in the optic nerve. **(d1-d4)** High magnification images of insets in **(d)**. Arrows in **(d3)** point to long distance regenerating axons. Arrows in **(d4)** point to regenerating axons in the optic chiasm. **(e-m)** Images of CT β -labeled, GFP-immunostained coronal sections of brain from CoCH GFP⁺ animal showing vLGN **(e-g; inset g1)**, dLGN **(h-j; insets h1-j1; inset j1')**, and SC **(k-m; inset m1)**. Asterisk in **(d)** and **(d1)** is lesion site. Scale bar in **(d)** = 500 μ m; **(d3)** = 250 μ m; **(d4)** = 100 μ m; **(e-g)** = 100 μ m; **(g1)** = 20 μ m; **(h-j)** = 100 μ m; **(j1-i1)** = 50 μ m; **(j1')** = 20 μ m; **(k-m)** = 250 μ m; **(m1)** = 50 μ m.

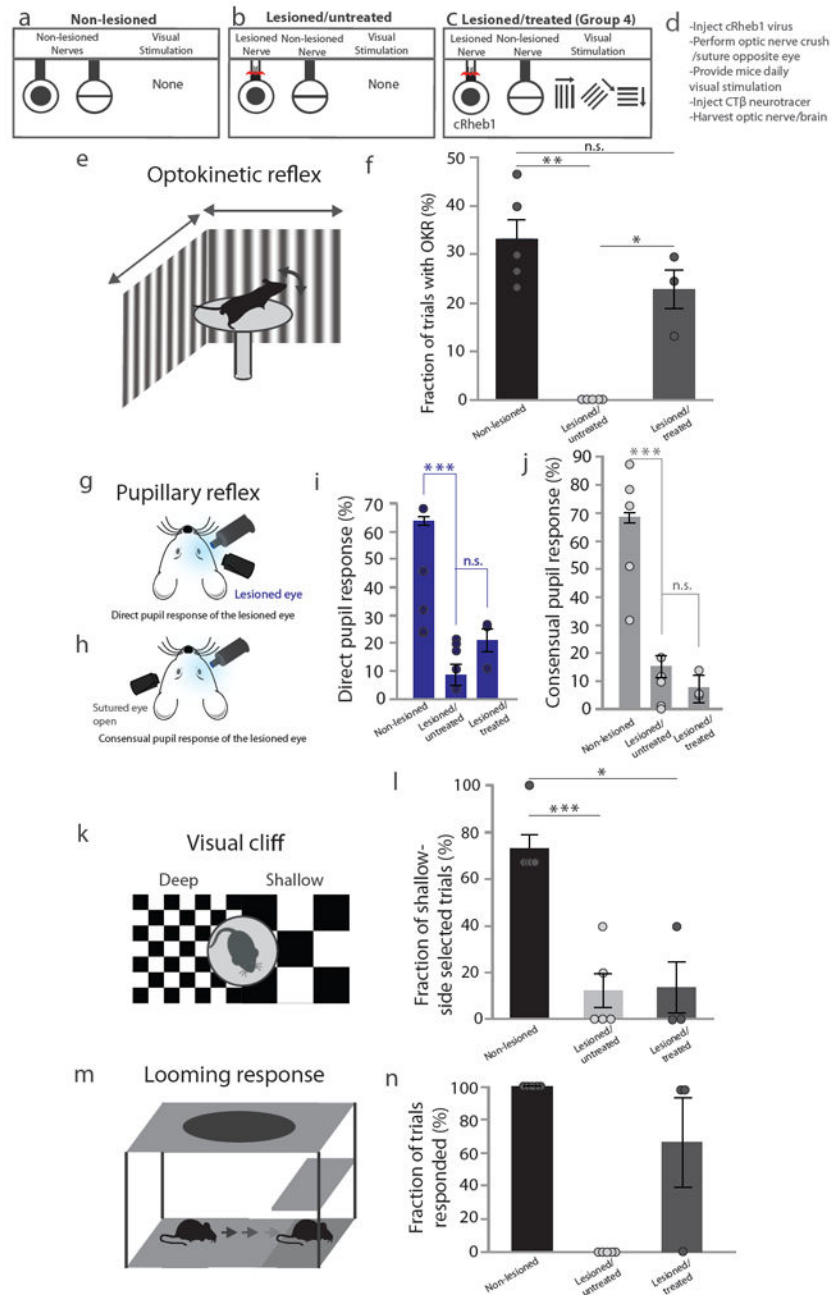


Figure 7. Combined daily visual stimulation and enhancement of mTOR signaling with cRheb1 overexpression partially rescues visually guided behaviors

(a-c) Schematics of the non-lesioned group ($n = 5$ mice) (a), lesioned and untreated group ($n = 5$ mice) (b), lesioned and treated group ('Group 4,' $n = 3$ mice) (c). (d) Summary of the experiments for the combined treatments. (e) Schematic of the optokinetic reflex behavior. (f) Bar graph of the mean percentage of the trials with optokinetic reflex (data presented as mean \pm SEM). Asterisks indicate statistical significance in unpaired one-tailed Student's t -test; * $P < 0.05$, ** $P < 0.005$ ($p = 0.0008$, $t = 7.67$, $dF = 4$; $p = 0.022$, $t = 4.613$, $dF = 2$; $p = 0.0857$, $t = 1.605$, $dF = 4.845$). (g) Schematic of the direct pupillary reflex response. (h) Schematic of the consensual pupillary reflex response. (i) Bar graph of the mean percentage

of the direct pupil constriction (data presented as mean \pm SEM). Asterisks indicate statistical significance in unpaired one-tailed Student's *t*-test; *** $P < 0.0005$ ($p < 0.0001$, $t = 13.03$, $dF = 5.862$; $p = 0.1712$, $t = 1.085$, $dF = 3.779$; $p = 0.0042$, $t = 7.927$, $dF = 2.443$). **(j)** Bar graph of the mean percentage of the consensual pupil constriction (data presented as mean \pm SEM). Asterisks indicate statistical significance in unpaired one-tailed Student's *t*-test; *** $P < 0.0005$ ($p < 0.0001$, $t = 14.55$, $dF = 6.207$; $p = 0.4799$, $t = 0.05594$, $dF = 2.327$; $p = 0.0193$, $t = 4.709$, $dF = 2.097$). **(k)** Schematic of the visual cliff behavior. **(l)** Bar graph of the mean percentage of the shallow side-selected trials (data presented as mean \pm SEM). Asterisks indicate statistical significance in unpaired one-tailed Student's *t*-test; * $P < 0.05$, *** $P < 0.0005$ ($p = 0.0002$, $t = 5.89$, $dF = 7.748$; $p = 0.4682$, $t = 0.08575$, $dF = 3.474$; $p = 0.0135$, $t = 4.025$, $dF = 3.03$). **(m)** Schematic of the looming response. **(n)** Bar graph of the mean percentage of the trials responded to looming stimulus (data presented as mean \pm SEM). Asterisks indicate statistical significance in unpaired one-tailed Student's *t*-test; ($p = 0.0918$, $t = 2$, $dF = 2$; $p = 0.2113$, $t = 1$, $dF = 2$).

Table 1
Targets innervated by regenerated RGC axons in each of the treatment conditions

Table summarizing the number of animals in each group with regenerated RGC axons to different visual nuclei. Control group is highlighted in blue. The two groups with combined biased visual stimulation with AAV2-cRheb1 are highlighted in red. Note that only these two groups showed regenerated RGC axons that re-innervated visual nuclei of in the brain.

Group	Animals	rostral ----- caudal									
		OC	SCN	vLGN	dLGN	OPN	MTN	NOT	SC		
1	<i>n</i> = 16	0/16	0/16	0/16	0/16	0/16	0/16	0/16	0/16	0/16	0/16
2	<i>n</i> = 5	0/5	0/5	0/5	0/5	0/5	0/5	0/5	0/5	0/5	0/5
3	<i>n</i> = 13	0/13	0/13	0/13	0/13	0/13	0/13	0/13	0/13	0/13	0/13
4	<i>n</i> = 10	7/10	5/10	6/10	6/10	6/10	6/10	6/10	5/10	6/10	6/10
5	<i>n</i> = 6	0/6	0/6	0/6	0/6	0/6	0/6	0/6	0/6	0/6	0/6
6	<i>n</i> = 5	1/5	0/5	0/5	0/5	0/5	0/5	0/5	0/5	0/5	0/5
7	<i>n</i> = 5	0/5	0/5	0/5	0/5	0/5	0/5	0/5	0/5	0/5	0/5
8	<i>n</i> = 5	0/5	0/5	0/5	0/5	0/5	0/5	0/5	0/5	0/5	0/5
9	<i>n</i> = 5	0/5	0/5	0/5	0/5	0/5	0/5	0/5	0/5	0/5	0/5
10	<i>n</i> = 9	6/9	4/9	5/9	5/9	4/9	4/9	4/9	4/9	4/9	6/9

Group 1 = no treatment/saline/AAV2-Cre
Group 2 = visual stimulation
Group 3 = AAV2-cRheb1
Group 4 = AAV2-cRheb1/suture opposite eye/visual stimulation
Group 5 = AAV2-cRheb1/visual stimulation
Group 6 = AAV2-cRheb1/suture opposite eye
Group 7 = AAV2-cRheb1/suture same eye/visual stimulation
Group 8 = Suture opposite eye/visual stimulation
Group 9 = Suture opposite eye
Group 10 = AAV2-cRheb1/remove opposite eye/visual stimulation